Enhancing Complementary Split Ring Resonators Performance for Atherosclerosis Diagnosis

Joséphine Masini, Frédérique Deshours, Georges Alquié, Olivier Meyer, Sylvain Feruglio, Dimitri Galayko, Hamid Kokabi, Jean-Michel Davaine

Enhancing Complementary Split Ring Resonators Performance for Atherosclerosis Diagnosis

Joséphine Masini Dupeyron*‡, Frédérique Deshours*, Georges Alquié*, Olivier Meyer*, Sylvain Feruglio‡, Dimitri Galayko‡, Hamid Kokabi* and Jean-Michel Davaine†

*Group of Electrical Engineering of Paris (GeePs), Sorbonne Université, CNRS UMR8507, F-75005 Paris, France
‡Laboratoire d'Informatique de Paris 6 (LIP6), Sorbonne Université, CNRS UMR7606, F-75005 Paris, France
†Service de chirurgie vasculaire, Pitié Salpêtrière, Sorbonne Université, F-75013 Paris, France

Email : josephine.masini@sorbonne-universite.fr

***Abstract*— This paper presents an improved complementary split ring resonator (CSRR) used as a non-invasive microwave sensor for in-vivo detection of atherosclerotic plaques. The sensor geometry was optimized on low-loss substrates to enhance the trade-off between the energy stored in the resonator and the energy radiated into the biological tissue. For positioning on the patient's neck, the sensors were simulated in the presence of multilayer structures, and animal tissue samples were used for validation to estimate the penetration depth of the electromagnetic waves in these tissues. Finally, a three-dimensional model of the carotid artery was developed to extend the analysis beyond the tissues of the neck. The simulated results offer promising prospects for in-vivo diagnosis of carotid atherosclerotic plaques using these optimized CSRRs.**

Keywords*— *carotid plaque, dielectric characterization, microwave sensor, sensitivity

I. Introduction

Due to their electromagnetic (EM) properties, various types of planar microwave sensors based on metamaterials are employed in medical applications for detection purposes (remote vital sign, breast cancer, brain stroke, blood glucose level, etc.) [1-2]. Metamaterials facilitate the design of compact and high-sensitivity resonant elements while operating at relatively low frequencies, thereby minimizing the cost of the associated electronics [3]. Complementary split ring resonators (CSRRs) are particularly sensitive to the dielectric properties of the materials. By measuring the changes in frequency and amplitude of the resonant peak induced by interaction with a dielectric material, they can be used to characterize the dielectric properties of the sample [4]. Previous studies have demonstrated the potential utility of CSRRs for diagnosing atherosclerosis [5]. Their ability to distinguish high-risk soft carotid atheromatous plaques (rich in necrosis and lipids) from highly calcified carotid plaques, considered stable and therefore less risky, was demonstrated by ex-vivo measurements carried out on around forty samples. An application with a very high clinical impact would therefore be non-invasive in-situ analysis of the composition of atheromatous plaques in the carotid artery for diagnosis [6].

For detection, the choice of resonator topology and resonant element plays a crucial role in sensor performance, particularly in terms of sensitivity, resolution, and dynamic range [7-8]. In applications involving multiple quantities to be measured, different sensitivities, including cross-sensitivities, can be defined. Consequently, drawing conclusions regarding the impact of resonator geometry on sensitivity and resolution proves exceedingly complex. This complexity makes determining the "optimal" resonator challenging [8]. Nevertheless, certain significant trends can be leveraged to optimize sensor structure. For instance, in the case of dielectric characterization, the real part of the complex permittivity of the tested material primarily affects the resonant frequency of the sensing element (through capacitive effects), while the imaginary part (related to the loss tangent) mainly influences the quality factor and the amplitude of the resonance peak. For a given resonator, optimizing these "natural" sensitivities yields valuable insights, particularly regarding substrate selection, operating frequency, and resonator geometry.

This article presents the results of a study conducted jointly on the frequency and amplitude sensitivity of a sensor initially developed from a classical CSRR, aiming to enhance the in-vivo detection and identification of atheromatous plaques located at the carotid bifurcation. Optimizations carried out using Ansys HFSS (High Frequency Structure Simulation Software) focused particularly on substrate selection and CSRR geometry to have a large contact surface with the sample, while maintaining a sufficiently high resonant frequency. New sensors were simulated in the presence of multilayer structures like those encountered in-vivo to reach the carotid artery, then fabricated and tested with animal-derived tissues (skin, fat, and muscle). Finally, a three-dimensional (3D) model of the carotid artery encapsulated in a multilayered tissue phantom mimicking the human neck was developed to assess the sensitivity of these new microwave sensors in detecting the presence of atheroma.

II. Sensitivity Analysis

For the measurement of dielectric properties, the input variable is the complex relative dielectric permittivity of atheromatous plaques, and the output variables are the characteristics of the resonance peak of the band-stop detection structure (resonant frequency, amplitude, quality factor). The typical topology and equivalent electrical circuit of the loaded CSRR are depicted in Fig. 1 [9-10]. C_C represents the coupling capacitance between the access line and the CSRR, L is the inductance of the feed line located above the resonator, $C_R^{'}$ is the capacitance of the CSRR loaded by the material, and L_R is the inductance of the CSRR unaffected by the material.

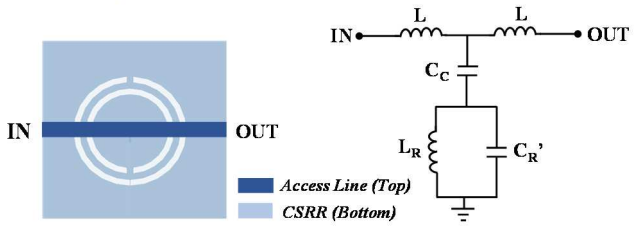

Fig. 1. Classical Topology of a CSRR and equivalent electrical circuit of the loaded resonator.

A. *Frequency Sensitivity*

The sensitivity of the CSRR is defined as the derivative of the resonant frequency (f_0) with respect to the relative permittivity of the matériel under test (ε_{rs}). To ensure a common basis for comparison for sensors operating by frequency variation, the relative sensitivity (S_r) is defined as follows [11-12]:

$$S_r = \frac{1}{f_0} \times \frac{df_0}{d\varepsilon_{rs}} \tag{1}$$

Assuming that the sample is in the region of the resonator where the electric field is most intense, a variation in the relative permittivity of the material will alter the capacitance of the CSRR, thereby causing a shift in the resonant frequency. Thus, the relative sensitivity can be expressed as follows [11-12]:

$$S_r = \frac{1}{f_0} \times \frac{df_0}{dC_R^{'}} \times \frac{dC_R^{'}}{d\varepsilon_{rs}} \tag{2}$$

with:
$$f_0 = \frac{1}{2\pi} \times \frac{1}{\sqrt{L_R\left(C_C + C_R^{'}\right)}} \tag{3}$$

Considering a semi-infinite uniform material in contact with the resonant element, a uniform and sufficiently thick substrate, and perfect metallization, the capacitance $C_R^{'}$ of the loaded resonator is given by [11-12]:

$$C_R^{'} = C_R \times \frac{\varepsilon_r + \varepsilon_{rs}}{\varepsilon_r + 1} \tag{4}$$

where C_R is the capacitance of the unloaded CSRR and ε_r is the relative permittivity of the substrate used for sensor design.

Deriving equation (3) with respect to capacitance $C_R^{'}$ and equation (4) with respect to ε_{rs}, we finally obtain:

$$S_r = -\frac{1}{2} \times \frac{C_R}{C_C\left(\varepsilon_r + 1\right) + C_R\left(\varepsilon_r + \varepsilon_{rs}\right)} \tag{5}$$

This formula demonstrates the advantage of designing resonators with a substrate of low dielectric constant, as it tends to reduce the coupling capacitance. However, ensuring good coupling between the line and the resonator is necessary to achieve a sufficient radiated field.

B. *Amplitude Sensitivity*

After simplification, the calculation of the minimum of the transmission coefficient magnitude (S_{21}) is given by:

$$|S_{21}|_{min} \approx \frac{1}{1 + \frac{\left(2\pi f_0\right)^2 \times C_C^2 \times R_r \times Z_0}{2}} \tag{6}$$

where R_r represents the losses of the resonator.

Since $|S_{21}|_{min}$ is inversely proportional to the square of the resonant frequency, the amplitude of the resonance peak will decrease with frequency, for a given substrate. Conversely, lower frequencies increase amplitude sensitivity and quality factor, allowing precise detection of small frequency variations, but reduce frequency sensitivity. Therefore, it is essential to find a compromise between geometry and dielectric losses by tuning the sensor's shape and selecting an appropriate substrate.

III. Design of Optimized Sensors

In the context of in-vivo measurements, the microwave signal needs to pass through a multilayer structure composed of skin, fat, and muscle. To enhance the penetration of electromagnetic waves into these tissues, the microwave sensor originally designed on FR4 substrate ($\varepsilon_r = 4.6$, $\tan\delta = 0.02$ at 10MHz) and used in our research on the dielectric characterization of atheromatous plaques has been modified accordingly.

A. *Choice of Substrate*

As previously discussed, enhancing sensor frequency and amplitude sensitivity involves using a substrate with low relative permittivity and minimal losses. Two improved substrates were therefore selected for comparison: the Rogers RO4003C™ ($\varepsilon_r = 3.38$, $\tan\delta = 0.0027$ at 10GHz) with a thickness of 0.81mm and the Rogers RT/duroid®5880 ($\varepsilon_r = 2.2$, $\tan\delta = 0.0009$ at 10GHz) with a thickness of 0.79mm. The metallizations are made of copper, with a thickness of 35µm and a conductivity of $5.8\times10^7 S.m^{-1}$.

B. *Access Line Topology and Resonator Geometry*

The microstrip feeding line has been widened at the coupling region with the resonator (Fig. 2.a). This low characteristic impedance line discontinuity (around 10Ω) acts as a reflector, reducing the energy radiated in the near field into the air. Consequently, it contributes to a better localization of energy within the substrate and the resonator.

To enhance the energy radiated into the biological tissues, a split ring and a circular slot positioned at the center of the CSRR have been added to the initial resonant structure described in [5] (Fig. 2.b). The contact surface with the sample remains approximately the same.

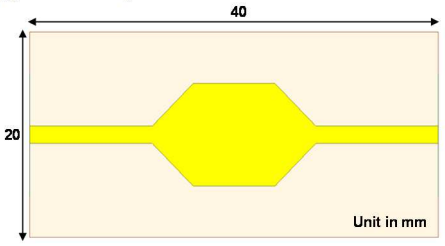

(a)

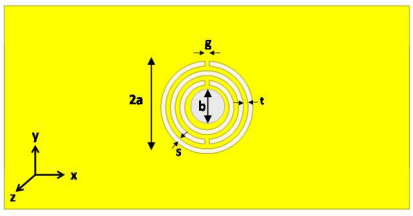

(b)

Fig. 2. Topology of the microwave sensor structure: (a) Widened feeding line (b) Ground plane engraved with the CSRR.

C. *Simulation and Measurement of Unloaded CSRRs*

Two new resonant sensors at different frequencies were fabricated using laser engraving, one on RT/duroid® 5880 (referred to as CSRR1) and the other on RO4003C™ (referred

to as CSRR2). To prevent short circuits between the CSRR rings due to residual moisture in the biological tissues, a 120µm thick glass plate was placed on each CSRR. This glass plate was accounted for in the simulation. Their dimensions and characteristics (resonant frequency f_0^{air} obtained for air, $|S_{21}|$ at f_0^{air}, and quality factor Q) are given in Table 1.

TABLE I. PARAMETERS OF THE SENSORS

Parameter	CSRR1	CSRR2
a (mm)	4.54	3
g = s = t (mm)	0.48	0.45
b (mm)	1.5	0.5
f_0^{air} (GHz)	2.404	3.882
$\|S_{21}\|$ (dB)	-32.1	-18.2
Q	167	104

Fig. 3 shows the transmission response of the two unloaded CSRRs between 1GHz and 5GHz. A 50MHz frequency deviation is observed between the measured and simulated values of f_0^{air}, mainly due to the sensor fabrication (engraving process accuracy: ±30 µm). The new CSRRs exhibit improved quality factors (167 and 104, respectively) compared to the original resonator (Q = 60) [5], enhancing the accuracy of dielectric parameter measurements for high-loss materials. With sharper resonance peaks, the resolution is improved, ensuring more precise determination of resonant frequencies and better assessment of frequency shifts induced by the samples. This provides an advantage in exploring tissues in greater depth.

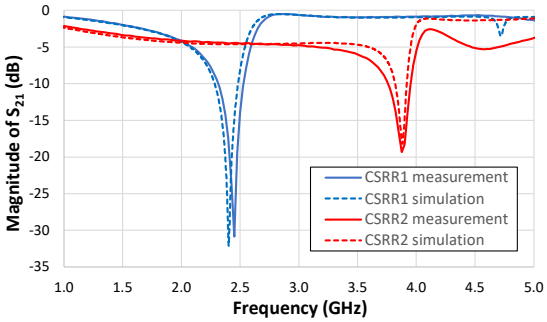

Fig. 3. Comparison between simulated and measured magnitude of S_{21}.

D. Estimation of CSRRs Sensitivy

The normalized frequency sensitivity (S_{norm}) of the sensors is depicted in Fig. 4 for ε_{rs} values ranging from 5 to 60 and for a tissue thickness of 4mm, as given by the following formula:

$$S_{norm} = 100 \times \frac{\Delta f}{f_0 \times (\varepsilon_{rs} - 1)} \quad (8)$$

where $\Delta f = f_0^{air} - f_0$ is the difference between the resonant frequencies of the unloaded and loaded CSRR, (ε_{rs}-1) being the relative variation of permittivity.

The simulation results in Fig. 4 confirm that the most frequency sensitive CSRR is the one designed on the substrate with the lowest relative permittivity (CSRR1 on RT/duroid® 5880). Taking total transmission ($|S_{21}| = 1$) as a reference, this CSRR, designed at a lower frequency, exhibits better relative amplitude difference and a reduced saturation effect at higher ε_{rs} values (Fig. 4).

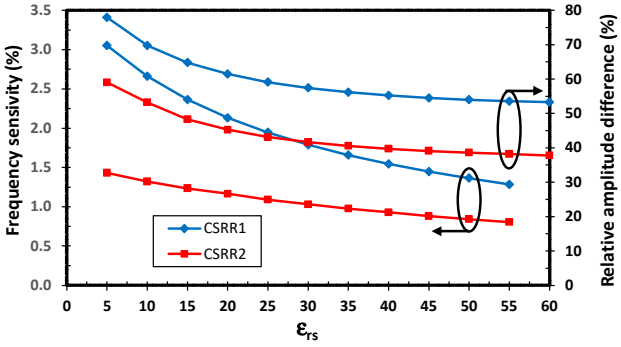

Fig. 4. Frequency sensitivity and relative amplitude difference versus ε_{rs}.

IV. RESULTS AND DISCUSSION

A. Measurements of Monolayers and Multilayers

The CSRRs were simulated in the presence of single-layer materials (skin, fat, muscle), and the validation of the results was carried out on tissue samples of animal origin. The thicknesses of the samples correspond to typical values of the tissues constituting the human neck: the thickness of the skin was 2mm, the fat 4mm, and the muscle 3mm. Table 2 summarizes the measured ε_{rs} values for the three single-layer samples, with satisfactory relative deviations ($\Delta\varepsilon$) calculated relative to the reference databases. Then, these samples were assembled to study multilayer structures like those of the human neck (skin+fat+muscle) and measured. The resonant frequency measurements showed significant frequency shifts between the skin-only sample and the multilayer structures. These shifts were confirmed by simulation and demonstrate adequate penetration of electromagnetic waves through multilayers.

TABLE II. EXPERIMENTAL RESULTS OF MONOLAYERS AND MULTILAYERS

Sensor	Tissue	Δf (MHz)	ε_{rs}	$\Delta\varepsilon$ (%)
CSRR1	Skin	880	32	13.5
	Fat	380	6.6	12
	Muscle	1100	50.7	6
	Multilayer	900	28	N.A.
CSRR2	Skin	1186	45.6	-23
	Fat	505	7.9	-5.5
	Muscle	1525	58.9	-9
	Multilayer	1453	38	N.A.

B. Simulation of atherosclerotic plaques in arteries

A 3D model of the carotid artery was implanted in HFSS, and the response of the sensors was simulated, considering the different tissues (skin, fat, muscle, and connective tissue) along the path of the EM waves. The carotid bifurcation, measuring 35mm in length, includes the common carotid artery (CCA), the internal carotid artery (ICA), and the external carotid artery (ECA) with respective diameters of 8mm, 5.6mm, and 4.6mm, all encapsulated in homogeneous connective tissue (Fig. 5). In a simplified approach, the presence of an atheroma located beneath the microwave sensor is modeled by varying the thickness and dielectric permittivity of the artery sheath. This allows for adjusting the obstruction level based on the simulation parameters.

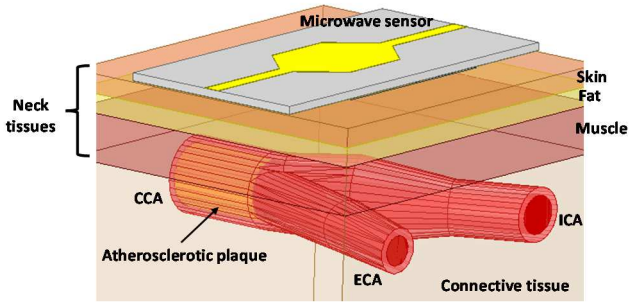

Fig. 5. 3D schematic of the carotid artery bifurcation model in HFSS.

Fig. 6 illustrates the profile of the normalized electric field radiated by the two CSRRs through the multilayer structure to the healthy artery in the (y0z) plane. The simulated results show that CSRR1 allows better penetration of the waves into the tissues. The EM waves are attenuated by approximately 50dB when they reach the artery.

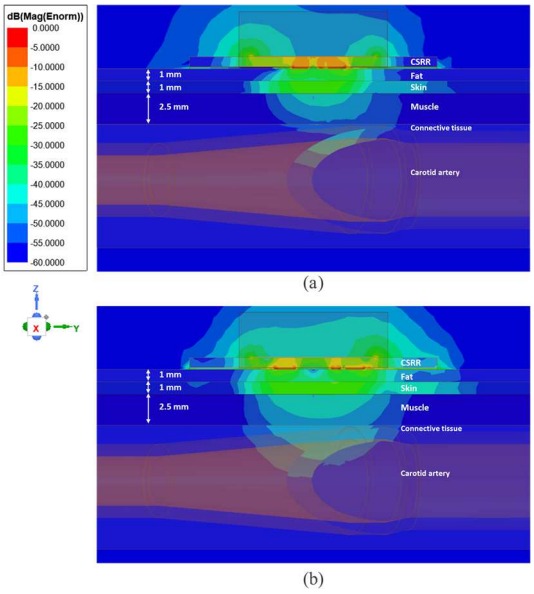

Fig. 6. Distribution of the electric field radiated in the (y0z) plane by (a) CSRR1 and (b) CSRR2 loaded with the neck tissues and the carotid artery.

Using the resonant frequency from a healthy artery (containing blood) as the reference, the frequency shift is simulated when a stable or vulnerable atherosclerotic plaque is introduced into the artery. The obtained results for the CSRR1 are represented in Fig. 7 as a function of atheroma plaque thickness, varying from 0.5 to 2.5mm. This range corresponds to degrees of stenosis between 12.5% and 62.5%. The simulation accuracy is estimated to be 0.5MHz.

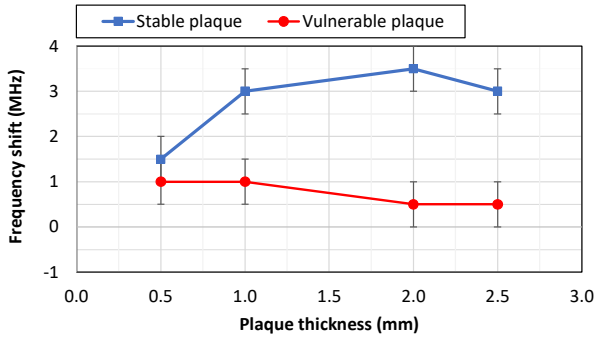

Fig. 7. Simulated frequency shift as a function of atheroma thickness.

Stable plaques with lower dielectric permittivity ($\varepsilon_{rs} = 10$) are better detected by the sensor, especially when the thickness of the atheroma is substantial. For a vulnerable plaque with a dielectric permittivity of 46, close to that of the artery sheath ($\varepsilon_{rs} = 42.6$), the frequency shift is significantly reduced, making detection difficult.

V. Conclusion

Two CSRR structures have been optimized to achieve high electric fields in biological tissues. The relevant parameters that can be adjusted relate to the geometry of the structure and the permittivity of the substrate on which they are designed. The sensitivity study of these sensors has been confirmed both by electromagnetic simulation and by measurements conducted on tissues of animal origin. The results obtained from multilayer configurations demonstrate significant wave penetration with one of the two CSRRs. The next step will be to perform in-vivo measurements to attempt detecting atherosclerotic plaques in the carotid artery. Additionally, future improvements will focus on enhancing sensor sensitivity to increase the frequency shift between stable and vulnerable plaques, thereby enabling more accurate plaque identification.

References

[1] C. Origlia, DO. Rodriguez-Duarte, JA. Tobon Vasquez, J-C Bolomey and F. Vipiana, “Review of Microwave Near-Field Sensing and Imaging Devices in Medical Applications,” in Sensors. 2024, 24(14):4515.

[2] J-C. Chiao et al., “Applications of Microwaves in Medicine,” in IEEE Journal of Microwaves, vol. 3, no. 1, pp. 134-169, Jan. 2023.

[3] A. Raj, A.K. Jha, M.A.H. Ansari, M.J. Akhtar and S. Panda, “Metamaterial-inspired microwave sensor for measurement of complex permittivity of materials,” in Microw. Opt. Technol. Lett., 58: 2577-2581, 2016.

[4] M. A. H. Ansari, A.K. Jha and M.J. Akhtar, “Design and application of the CSRR-based planar sensor for non-invasive measurement of complex permittivity,” in IEEE Sensors J., vol. 15, no. 12, pp. 7181-7189, Dec. 2015.

[5] R. Shahbaz, et al., “Identification of Carotid Plaques Composition Through a Compact CSRR-Based Microwave Sensor,” in IRBM 2022, p. 100734.

[6] R. Shahbaz, et al., “In vitro analysis of carotid lesions using a preliminary microwave sensor to detect vulnerable plaques: Correlation with histology, Duplex ultrasound examination, and computed tomography scanner: The Imaging and Microwave Phenotyping Assessment of Carotid stenosis Threat (IMPACT) study,” in JVS-Vascular Science, vol. 5, 100182, 2024.

[7] M. Durán-Sindreu, J. Naqui, F. Paredes, J. Bonache and F. Martín, “Electrically small resonators for planar metamaterial, microwave circuit and antenna design: A comparative analysis,” in Appl. Sci. 2012, 2, 375–395.

[8] J. Muñoz-Enano, P. Vélez, M. Gil and F. Martín, “Planar Microwave Resonant Sensors: A Review and Recent Developments,”in Appl. Sci. 2020, 10(7):2615.

[9] D. Baena et al., “Equivalent-circuit models for split-ring resonators and complementary split-ring resonators coupled to planar transmission lines,” in IEEE Transactions on Microwave Theory and Techniques, vol. 53, no. 4, pp. 1451-1461, April 2005.

[10] J. Bonache, M. Gil, I. Gil, J. Garcia-Garcia and F. Martin, “On the electrical characteristics of complementary metamaterial resonators,” in IEEE Microwave and Wireless Components Letters, vol. 16, no. 10, pp. 543-545, Oct. 2006.

[11] F. Martín, P. Vélez, J. Muñoz-Enano and L. Su, “Planar Microwave Sensors,” September 2022, Wiley-IEEE Press.

[12] M. Abdolrazzaghi, V. Nayyeri and F. Martin, “Techniques to improve the performance of planar microwave sensors: a review and recent developments,” in Sensors 2022, 22, 6946.